The 8th European Congress on Computational Methods in Applied Sciences and Engineering
ECCOMAS Congress 2022
5 – 9 June 2022, Oslo, Norway

USING ARTIFICIAL INTELLIGENCE TECHNIQUES FOR THE ACCURATE ESTIMATION OF THE ULTIMATE PURE BENDING OF STEEL CIRCULAR TUBES

MOHAMED EL AMINE BEN SEGHIER [1*], VAGELIS PLEVRIS[2] AND GERMAN SOLORZANO[3]

[1] Department of Building and Real Estate, Faculty of Construction and Environment,
Hong Kong Polytechnic University, Hung Hom, Kowloon, Hong Kong
email: mohamed.benseghier@polyu.edu.hk

[2] Department of Civil and Architectural Engineering,
Qatar University, P.O. Box: 2713, Doha, Qatar
email: vplevris@qu.edu.qa

[3] Department of Civil Engineering and Energy Technology,
OsloMet—Oslo Metropolitan University, 0167 Oslo, Norway
email: germanso@oslomet.no

Key words: Artificial intelligence; Ultimate pure bending capacity; Circular tubes; Statistical index; Taylor Diagram

Abstract. In this paper, the potential of building more accurate and robust models for the prediction of the ultimate pure bending capacity of steel circular tubes using artificial intelligence techniques is investigated. Therefore, a database consisting of 104 tests for fabricated and cold-formed steel circular tubes are collected from the open literature and used to train and validate the proposed data-driven approaches which include the Random Forest methodology in two variants: the original version in which the control parameters are manually updated, and an enhanced RF-PSO variant, where Particle Swarm Optimization is used for optimizing these parameters. The data set has four input parameters, namely the tube thickness, tube diameter, yield strength of steel and steel elasticity modulus, while the ultimate pure bending capacity is considered as the target output variable. The obtained results are compared to the real test values through various statistical indicators such as the root mean square error and the coefficient of determination. The results indicate that the proposed enhanced model can provide an accurate solution for modelling the complex behavior of steel circular tubes under pure bending conditions.

1 INTRODUCTION

Circular steel tubes represent one of the most popular structural profiles used in the steel construction industry. Their double symmetry makes them particularly well suited for resisting bending stresses in any direction simultaneously [1]. As a result, they are usually one of the most economical alternatives for structural members that are subjected to various types of loading conditions, such as the case of columns or pipes. When circular steel tubes experience

large stresses on their cross-section, their deformation mechanism is characterized by a physical phenomenon referred to as “ovalization” [2]. This phenomenon has to do with the progressive deformation of the circular cross section into an oval-like shape. Consequently, the stiffness and the geometrical properties of the section change drastically resulting in a highly non-linear structural response [3]. Such a mechanism could lead to severe damage or complete failure that could result in severe environmental and economic loses. For this reason, it is of particularly high importance to find appropriate and reliable mathematical models to study the behavior of these structural elements in detail.

Scientists and engineers have proposed various close-form solutions to estimate the bending moment capacity of circular steel tubes which are usually based on thorough experimental testing [4-10]. Among the most established and frequently used methods are those that are included in building design codes such as Eurocode 3 [11], AS/NZS 4600 [12], AS 4100 [13] and AISC [14]. However, most of these estimations assume that the deformed, ovalized shape is a perfect ellipse [15] which may not be accurate, especially in the case of large deformations. More advanced models with the inclusion of plastic hinges at specific points [16], or along the whole element length [1] have also been proposed. These methods can estimate the bending capacity considering higher degrees of ovalization with sufficient accuracy for practical purposes. Nevertheless, the most reliable models are highly detailed finite element models using appropriated plasticity constitutive laws and considering the geometric non-linearity in their formulation [17]. Such detailed models are capable of simulating both small and large degrees of ovalization, and even some other difficult physical phenomena, such as self-contact [18]. However, they are commonly used only for research purposes due to their heavy computational cost and the difficulty in their formulation and implementation.

Although some of the previously mentioned mathematical models are capable of estimating the bending capacity of steel circular tubes, their applicability is limited because of the assumptions used in their formulations, or in the case of complex FE models, because of their heavy computational cost which poses simulation challenges [19]. On the other hand, data-driven Artificial Intelligence (AI) methods offer much more flexibility as they do not require any assumptions and are able to estimate the bending capacity by directly interpolating from the available testing data with sufficient accuracy and with a considerably low computational effort.

AI-driven methodologies have become very popular in solving practical engineering problems in the last decade. For example, problems related to masonry structures [20-22], degradation in steel structures [23, 24], concrete structures [25, 26], steel structures [27, 28], optimal cost-design of concrete footings [29] and other interesting and novel applications [30]. In terms of the estimation of the bending capacity of steel circular tubes , Shahin and Elchalakani [31] utilized artificial neural networks (ANNs) for this purpose, outperforming the estimations from the formulas in current building codes. Basarir et al. [32] used neuro-fuzzy inference algorithms and neural networks to predict the bending capacity of concrete-filled tubes, demonstrating the significant advantages of AI-based models compared to the traditional mathematical approaches.

In this paper, we investigate various hybrid-AI methodologies based on the random forest (RF) methodology, for estimating the ultimate bending capacity of circular steel tubes. The RF technique is implemented in two variants: the original RF and an optimized RF using particle swarm optimization (PSO). The proposed models are trained and tested on an experimental

database before being evaluated using various performance metrics. The structure of the paper is as follows: Sections 2 presents the collected data and the proposed framework based on RF and PSO. Section 3 presents the results and the relevant discussion, while Section 4 summarizes the main conclusions of the work.

2 DATA AND IMPLEMENTATION

2.1 Database of circular steel tubes bending capacity

To build accurate models using artificial intelligence techniques, the use of a comprehensive database is of particular importance. In this regard, a database containing 104 experimental tests of circular steel tubes subjected to pure bending obtained from the open literature is used in this work to train and test the developed models. 47.1% of the experimental data is from fabricated tubes (49 experimental tests) and is labeled as F01 to F49 [4-8]), while the remainder 52.9% is from cold-form tubes (55 experimental tests) and is labeled as C01 to C55 [9, 10]. The information is gathered from a variety of sources, such as those listed in [4-10].

The target output is the ultimate bending capacity (UBC) of the steel tube, while the inputs are 4 parameters, namely (1) the section's thickness t, (2) the section's diameter d, (3) the yielding stress of the fabrication steel f_y, and (4) the elastic modulus E of the material. All the relevant experimental data values are reported in Table 1. It should be noted that these data are randomly divided into two categories: training data (80%) for creating the models, and testing data (20%) for testing the performance of the generated models.

Table 1: Experimental test results: Fabricated tubes [4-8] and cold-formed circular tubes [9, 10].

ID	Inputs				Output	ID	Inputs				Output
	t (mm)	d (cm)	f_y (MPa)	E (GPa)	M_u (kN·m)		t (mm)	d (cm)	f_y (MPa)	E (GPa)	M_u (kN·m)
F01	26.6	45.7	279	199.63	1442.1	**C01**	2.53	10.18	365	199.80	8.8
F02	18.7	45.7	299	199.90	1237.0	**C02**	2.6	8.86	432	209.50	8.0
F03	16.5	45.8	338	200.36	1198.1	**C03**	2.45	7.63	415	217.10	5.1
F04	13.1	45.8	299	200.35	830.9	**C04**	3.35	8.93	412	217.90	9.9
F05	9.9	45.8	294	200.59	562.9	**C05**	2.44	6.06	433	211.10	3.1
F06	6.9	45.8	325	199.43	381.5	**C06**	3.24	7.62	456	211.10	7.6
F07	6.1	45.6	314	200.91	346.6	**C07**	3.01	6.06	408	204.70	4.2
F08	6.3	45.6	309	201.07	358.6	**C08**	1.98	3.36	442	204.20	0.8
F09	12.9	61.0	314	200.08	1490.1	**C09**	2.63	3.38	460	207.10	1.1
F10	6.8	61.0	373	201.20	810.4	**C10**	1.1	11.01	408	190.90	3.9
F11	25.4	45.7	374	199.94	1892.7	**C11**	1.0	10.99	408	190.90	3.7
F12	19.6	45.8	390	199.86	1408.6	**C12**	0.9	10.97	408	190.90	3.4
F13	18.8	45.5	367	198.94	1391.7	**C13**	1.25	11.04	408	190.90	4.5
F14	16.4	45.8	424	199.92	1302.9	**C14**	1.7	9.86	410	212.30	5.8
F15	13.3	45.8	411	199.93	1111.5	**C15**	1.2	9.88	404	191.20	4.3
F16	10.0	45.8	410	200.49	783.4	**C16**	1.4	9.92	404	191.20	4.9
F17	6.8	45.8	434	199.50	538.8	**C17**	1.6	9.96	365	199.80	5.4
F18	13.6	61.0	405	199.14	1729.7	**C18**	1.8	10.00	365	199.80	5.3
F19	13.7	60.8	378	199.72	1828.2	**C19**	2.3	9.98	410	212.30	8.9
F20	7.0	60.9	429	200.62	918.3	**C20**	2.4	8.73	412	217.90	5.7
F21	9.9	60.8	401	200.25	1317.2	**C21**	2.1	10.06	404	191.20	7.5
F22	14.9	27.3	290	210.00	306.1	**C22**	2.44	10.18	365	200.00	8.7

F23	7.8	27.3	304	210.00	160.0	**C23**	2.52	8.93	378	182.00	6.4
F24	5.6	27.3	405	210.00	150.9	**C24**	2.17	7.63	415	217.00	4.7
F25	4.9	27.3	419	210.00	139.7	**C25**	3.1	8.93	412	218.00	9.4
F26	3.5	27.3	287	210.00	64.7	**C26**	2.23	6.07	433	211.00	3.0
F27	2.5	27.3	311	210.00	48.8	**C27**	3.07	7.62	456	211.00	7.7
F28	1.9	10.9	269	210.00	7.1	**C28**	2.9	6.07	408	205.00	3.7
F29	1.4	10.3	270	210.00	4.3	**C29**	2.4	3.38	460	207.00	1.1
F30	1.1	10.5	270	210.00	3.2	**C30**	2.44	10.18	365	200.00	8.4
F31	0.94	10.3	245	210.00	2.3	**C31**	2.44	10.18	365	200.00	8.7
F32	0.76	10.4	267	210.00	1.6	**C32**	2.52	8.93	378	182.00	6.7
F33	2.9	10.0	358	210.00	10.3	**C33**	3.08	8.91	473	201.00	10.0
F34	2.3	12.5	359	210.00	12.2	**C34**	2.29	6.02	407	211.00	3.3
F35	1.6	11.2	357	210.00	7.4	**C35**	3.07	7.62	456	211.00	7.4
F36	0.99	8.9	370	210.00	2.7	**C36**	2.95	6.04	413	196.00	4.0
F37	1.3	11.7	394	210.00	6.2	**C37**	2.54	10.11	400	190.00	10.5
F38	5.9	27.3	380	210.00	167.2	**C38**	2.52	8.93	378	182.00	7.2
F39	8.9	27.3	334	210.00	232.1	**C39**	2.35	7.61	370	202.00	4.6
F40	6.6	40.6	342	210.00	385.7	**C40**	3.08	8.91	473	201.00	10.6
F41	6.5	50.8	375	210.00	593.1	**C41**	2.29	6.02	407	211.00	3.3
F42	3.9	11.4	308	210.00	15.4	**C42**	3.13	7.59	402	198.00	6.7
F43	3.9	16.8	305	210.00	33.2	**C43**	2.95	6.04	413	196.00	4.3
F44	4.8	16.8	368	210.00	48.3	**C44**	2.52	8.93	378	182.00	7.3
F45	5.6	27.3	306	210.00	126.7	**C45**	2.29	6.02	407	211.00	3.8
F46	6.4	32.4	377	210.00	248.9	**C46**	2.95	6.04	413	196.00	4.6
F47	6.4	35.6	297	210.00	231.3	**C47**	2.54	10.11	400	190.00	8.7
F48	6.3	40.6	309	210.00	297.0	**C48**	2.52	8.93	378	182.00	6.4
F49	6.4	50.8	362	210.00	509.5	**C49**	2.35	7.61	370	202.00	4.3
						C50	3.08	8.91	473	201.00	9.8
						C51	2.29	6.02	407	211.00	3.3
						C52	3.13	7.59	402	198.00	5.9
						C53	2.95	6.04	413	196.00	4.1
						C54	2.52	8.93	378	182.00	6.2
						C55	2.95	6.04	413	196.00	4.0

2.2 Random Forest

Leo Breiman's Random Forest (RF) is a powerful Ensemble Learning (EL) approach that combines bagging ensemble learning theory [33] with Ho's random subspace method [34]. RFs are a combination of tree predictors such that each tree depends on the values of a random vector sampled independently and with the same distribution for all trees in the forest. A decision tree (DT) has the same basic structure as the RF for prediction problems, but it suffers from overfitting in cases where the input variables are complex and as a result DTs are unable to cope effectively with classification problems. Consequently, RF outperforms the standard DT model in terms of generalization and prediction accuracy [35]. The unpredictability of the RF model is most visible in the two aspects stated below. To begin, the bootstrap technique is used to generate *K* new sample sets randomly from the training set based on the model inputs, with each new sample set being used to train a DT. As a result, the basis estimator in the RF model is *K* DTs. The unselected samples make up the out-of-bag (OOB) databases. Second, during the DT construction, a certain number of features (*N*) from the input variables must be retrieved at random. For prediction purposes, each DT will generate an estimated result, and all

prediction results from the *K* DTs will be voted on to determine the final predicted RF outcome. The ultimate decision outcome of the RF model is calculated using Eq. (1) [36]:

$$H(\boldsymbol{X}) = \arg max \sum_{i=1}^{K} I(h_i(\boldsymbol{X}) = \boldsymbol{Y}) \quad (1)$$

where $H(\boldsymbol{X})$ denotes an RF model with various DTs; h_i is the *i*-th individual DT; *K* is the total number of DTs; and *X* and *Y* represent the vectors of the input variables and the correct prediction, respectively.

2.3 Particle Swarm Optimization

Particle swarm optimization (PSO) is a metaheuristic optimization algorithm that is based on the dynamic movements and social behavior that is observed in social animals such as bird flocks or schools of fishes. It was introduced by Kennedy and Eberhart [37] and since then it has been widely implemented for solving practical optimization problems in engineering and other disciplines [38-41]. The searching method of PSO iteratively updates a population (swarm) of possible solutions, which are known as "particles". Each particle is labeled with its location (i.e. coordinates) and velocity in the *D*-dimensional search space [42]. The particles' positions represent alternative solutions of the optimization problem, where at an iteration *k*, the relevant position and velocity for a particle *i* are expressed as follows:

$$\boldsymbol{X}_{i,k} = \{\boldsymbol{X}_{i1}, \boldsymbol{X}_{i2}, \dots, \boldsymbol{X}_{iD}\} \quad (2)$$

$$\boldsymbol{v}_{i,k} = \{\boldsymbol{v}_{i1}, \boldsymbol{v}_{i2}, \dots, \boldsymbol{v}_{iD}\} \quad (3)$$

where $\boldsymbol{v}_{i,k}$ and $\boldsymbol{x}_{i,k}$ denote the velocity and position of the *i*-th particle at iteration *k*, respectively. The velocity of each particle changes with the iterations according to Eq. (4) as follows:

$$\boldsymbol{v}_{i,k+1} = \chi * \left((\boldsymbol{v}_{i,k} + c_1 r_1 (\boldsymbol{pbest}_{i,k} - \boldsymbol{x}_{i,k}) + c_2 r_2 (\boldsymbol{gbest}_k - \boldsymbol{x}_{i,k})\right) \quad (4)$$

where $\boldsymbol{pbest}_{i,k}$ signifies the *i-th* particle's best position at the *k-th* iteration; $\boldsymbol{gbest}_k$ denotes the best position ever found by the entire swarm, while c_1 and c_2 are positive, predefined acceleration constants and r_1, r_2 are uniformly distributed random numbers in the range [0, 1]. The parameter χ, known as the convergence factor, is computed as follows

$$\chi = \frac{2}{\left|2-\theta-\sqrt{\theta^2-4\theta}\right|} \quad (5)$$

with $\theta = c_1 + c_2 > 4$. Commonly, θ is equal to 4.1, and as a result $\chi = 0.729$. Each particle changes its position at each iteration according to Eq. (6):

$$\boldsymbol{X}_{i,k+1} = \boldsymbol{X}_{i,k} + \boldsymbol{v}_{i,k+1} \quad (6)$$

Both $\boldsymbol{pbest}_i$ (for every particle i) and ***gbest*** (for the entire swarm) are updated at each iteration if a new location corresponds to an improved value of the objective function.

3 RESULTS AND DISCUSSIONS

Before presenting and discussing the results, the appropriate tools for evaluating the performance of the RF and RF-PSO **models** for predicting the ultimate bending capacity of circular steel tubes should be described. Thus, after obtaining the modeling results, the

following procedure is followed which takes into account three types of evaluation tools: **(**1) Statistical indicators, (2) Graphical indicators, and (3) The Taylor Diagram [43]. The first set of tools includes four statistical indicators: (i) Root mean squared error (RMSE), (ii) Relative root mean squared error (RRMSE), (iii) Mean bias error (MBE), and (iv) Mean absolute relative error (MARE). The mathematical expressions of these performance metrics are described in Eqs (7)-(10) as shown below,

$$RMSE = \sqrt{\frac{1}{n}\sum_{i=1}^{n}\left(UBC_i^{exp} - UBC_i^{pre}\right)^2} \tag{7}$$

$$RRMSE = \frac{\sqrt{\frac{1}{n}\sum_{i=1}^{n}\left(UBC_i^{exp} - UBC_i^{pre}\right)^2}}{\sum_{i=1}^{n} UBC_i^{exp}} \tag{8}$$

$$MBE = \frac{1}{n}\sum_{i=1}^{n}\left(UBC_i^{exp} - UBC_i^{pre}\right)^2 \tag{9}$$

$$MARE = \frac{1}{n}\sum_{i=1}^{n}\left|\frac{UBC_i^{exp} - UBC_i^{pre}}{UBC_i^{exp}}\right| \tag{10}$$

where $\boldsymbol{UBC_i^{exp}}$and $\boldsymbol{UBC_i^{pre}}$ are the experimental and predicted values of the ultimate bending capacity of circular steel tubes, respectively. It should be noted that in general, the lower the values of the metrics RMSE, RRMSE, MBE, and MARE, the better the model predictions.

The second evaluation tool is the graphical representation, which is used to compare the agreement between the experimental results (ground truth values) and the predicted values using the RF and RF-PSO prediction models. For this purpose, a scatterplot-based coefficient of determination (Eq.11) is used, as shown in Eq. (11),

$$R^2 = \left(\frac{\sum_{i=1}^{n}\left(\boldsymbol{UBC_i^{pre} - UBC_{avg}^{pre}}\right)\left(\boldsymbol{UBC_i^{exp} - UBC_{avg}^{exp}}\right)}{\sqrt{\sum_{i=1}^{n}\left(\boldsymbol{UBC_i^{pre} - UBC_{avg}^{pre}}\right)^2 \cdot \sum_{i=1}^{n}\left(\boldsymbol{UBC_i^{exp} - UBC_{avg}^{exp}}\right)^2}}\right)^2 \tag{11}$$

where $\boldsymbol{UBC_{avg}^{exp}}$and $\boldsymbol{UBC_{avg}^{pre}}$ are the mean values of the experimental and predicted values for the ultimate bending capacity of circular steel tubes, respectively.

The Taylor Diagram [43] is a globe-based graphical comparison tool that includes and combines three statistical indicators: (i) the (Centered) Root mean squared error, (ii) the standard deviation, and (iii) the Pearson correlation coefficient *R* (Eq. (12)), which is used as the last performance comparative tool in this study.

$$R = \frac{n\sum_{i=1}^{n}\left(\boldsymbol{UBC_i^{pre}.UBC_i^{exp}}\right) - \sum_{i=1}^{n}\left(\boldsymbol{UBC_i^{pre}}\right)\sum_{i=1}^{n}\left(\boldsymbol{UBC_i^{exp}}\right)}{\sqrt{\left[n\sum_{i=1}^{n}\left(\boldsymbol{UBC_i^{pre^2}}\right) - \left(\sum_{i=1}^{n}\left(\boldsymbol{UBC_i^{pre}}\right)\right)^2\right]\left[n\sum_{i=1}^{n}\left(\boldsymbol{UBC_i^{exp^2}}\right) - \left(\sum_{i=1}^{n}\left(\boldsymbol{UBC_i^{exp}}\right)\right)^2\right]}} \tag{12}$$

3.1 Statistical indicators results and discussion

Table 2 displays the results of the aforementioned statistical indicators, for the two phases of training and testing, as well as the overall results (training and testing, together). The results show that using the hybrid model, RF-PSO, provides the best performance when compared to the original RF model when using all indicators and for all phases. During the training and testing phases, RF-PSO achieved RMSE values of 96.40 kN·m and 148.04 kN·m, respectively.

This draws attention to the fact that the training phase is slightly better than the testing phase, which can be explained by the amount of data used for training the models (80%) compared to the amount of data used for testing the models (20%). Another point to note is the high values obtained by using the MBE statistical indicator, which can be attributed to the fact that this indicator is capable of accurately representing problems with relatively small values when compared to large value results. Overall, it is estimated that using PSO to optimize the RF control parameters yields better results in comparison to the simple RF model. Particularly, the RF metric values are larger than the corresponding RF-PSO values, by 40.2% for RMSE, 41.9% for RRMSE, 77.5% for MBE and 11.5% for MARE, as shown in Table 2.

Table 2: Results of the evaluation during the training, testing and overall phases.

		Proposed models	
Phase	**Indicator**	**RF**	**RF-PSO**
Training	RMSE	132.7186	96.3956
	RRMSE	0.7171	0.5208
	MBE	17614.2377	9292.1201
	MARE	0.9661	0.8794
Testing	RMSE	217.5238	148.0406
	RRMSE	2.5564	1.7398
	MBE	34420.1532	21916.0087
	MARE	1.1385	0.9674
Overall	RMSE	149.6797	106.7246
	RRMSE	1.0849	0.7646
	MBE	20975.4208	11816.8978
	MARE	1.0006	0.8970

3.2 Graphical analysis

To illustrate the agreement between the predicted results and the experimental (ground truth) values, the scatter plots are plotted in Figure 1 and Figure 2, for the RF and RF-PSO models, respectively, during the training and the testing phases. The coefficient of determination R^2 is included in each subfigure. In these figures, the black line represents the perfect agreement between the predicted and the experimental values, whereas the dashed red line represents the linear relationship between predicted and experimental values according to the linear regression model. It can be seen that during the training and testing phases, RF-PSO provides R^2 values of 0.9638 and 0.9392, respectively, compared to 0.9121 and 0.9125 for the corresponding values of the simple RF model, which indicates that the RF-PSO model is better than the RF model. In terms of R^2 values, the RF-PSO model outperforms the original RF model in the training and testing phases by 5.7% and 2.9%, respectively.

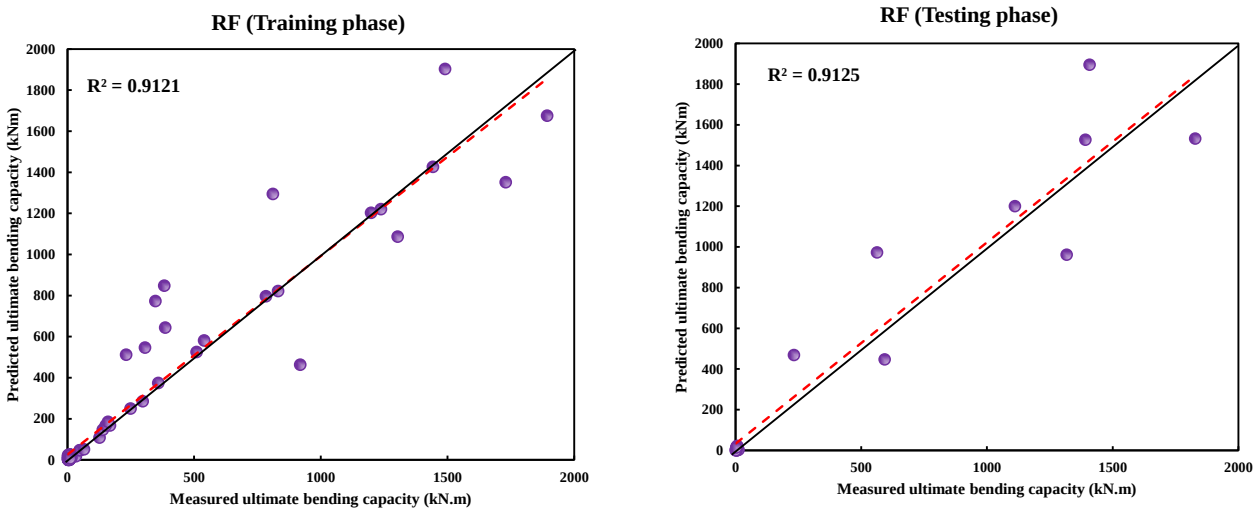

(a) (b)

Figure 1: Scatterplots of predicted vs experimental (ground truth) results, using RF: (a) Training phase, (b) Testing phase.

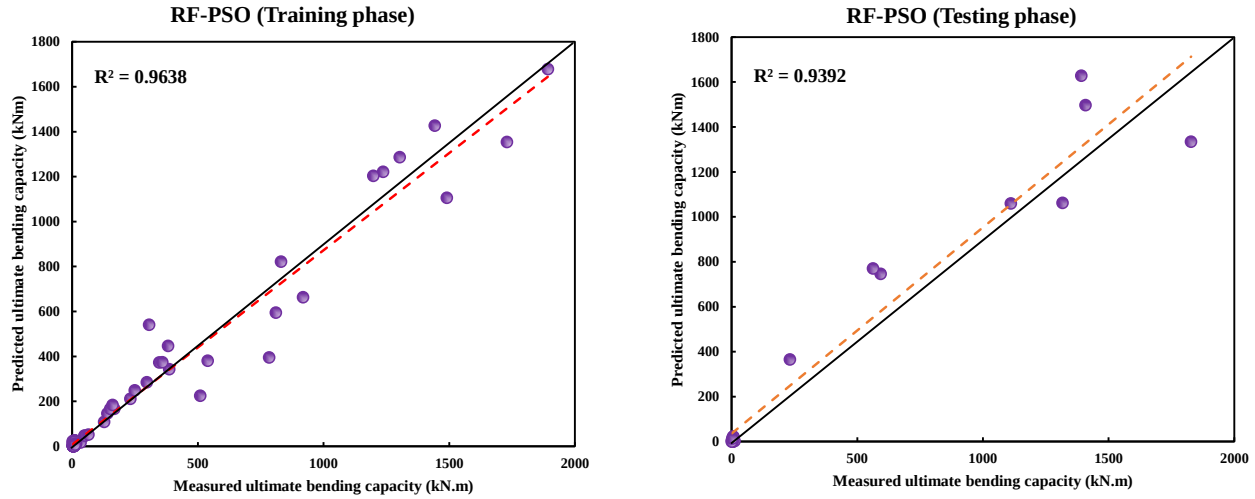

(a) (b)

Figure 2: Scatterplots of predicted vs experimental (ground truth) results, using RF-PSO: (a) Training phase, (b) Testing phase.

3.2 Taylor diagram

The Taylor diagram [43], can provide a global performance comparison based on multiple indicators. Figure 3 depicts the results of the Taylor diagram-based analysis for the training and testing phases. The standard deviations are defined by the dashed black circles, including the red dashed circle which corresponds to the standard deviation of the experimental values set. The Pearson correlation coefficient is defined by the gray straight line. The closer the obtained

model results point is to the real/experimental value point (full red circle), the better the model's overall performance in general. In both the training and the testing phases, the RF-PSO model results are the closest to the experimental results. In comparison to the original RF model, the proposed RF-PSO model has a higher Pearson correlation coefficient equal to 0.982 during the training phase and 0.969 during the testing phase, compared to 0.955 during both phases using the original RF model. Thus, it is shown that the use of meta-heuristic algorithms and in particular PSO can improve the performance of the original RF model when solving complex prediction problems such as the problem of estimating the ultimate bending capacity of circular steel tubes.

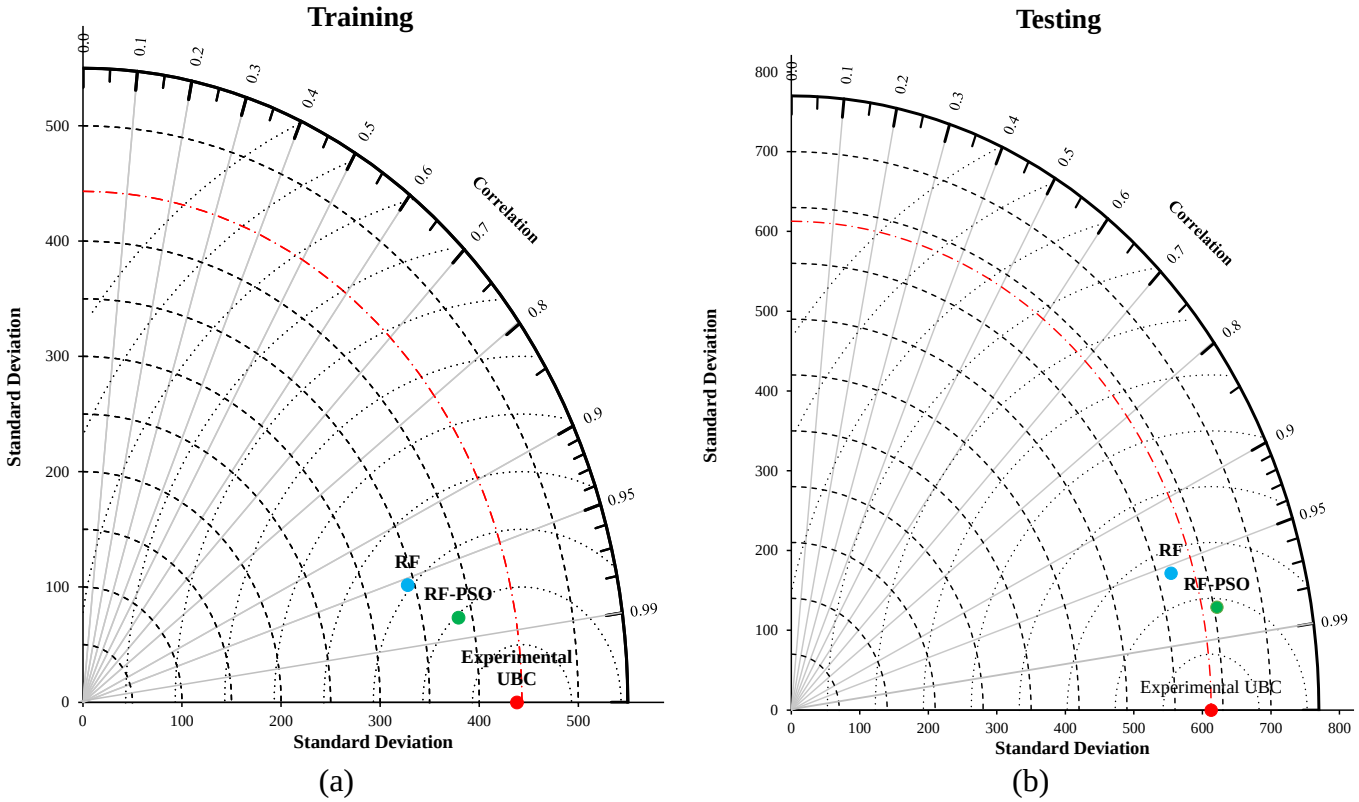

Figure 3: Taylor diagram for the RF and RF-PSO models: (a) Training phase, (b) Testing phase.

4 CONCLUSIONS

The behavior of steel tubes and in particular their ultimate bending capacity is modeled in this study using artificial intelligence models based on the random forest technique and particle swarm optimization. The proposed approach includes the original RF technique in which the control parameters are manually updated, as well as the new RF-PSO approach, where PSO is used for optimizing these parameters. Following that, a database of 104 samples extracted from the literature is used to train and test the models, with 80% of the data used for training and the remaining 20% used for testing. The performance of the models is evaluated using a variety of metrics, including four statistical indicators and graphical representations.

The results show that the proposed RF-PSO model outperforms the original RF in terms of accuracy and efficiency. In particular, the RF metric values are larger than the corresponding PSO-optimized RF model values, by 40.2% for RMSE, 41.9% for RRMSE, 77.5% for MBE and 11.5% for MARE. Furthermore, in terms of R^2 values, the RF-PSO model outperforms the original RF model in the training and testing phases by 5.7% and 2.9%, respectively. The study can be improved further by using more robust and powerful nature-inspired algorithms to improve the generalization and performance of the RF model. In addition, future research should investigate the impact of random database splitting on model performance, as well as the impact of input parameters on the target output.

REFERENCES

[1] Elchalakani, M., X.L. Zhao, and R.H. Grzebieta, *Plastic mechanism analysis of circular tubes under pure bending.* International Journal of Mechanical Sciences, 2002. **44**(6): p. 1117-1143 DOI: https://doi.org/10.1016/S0020-7403(02)00017-6.

[2] Chitawadagi, M.V. and M.C. Narasimhan, *Strength deformation behaviour of circular concrete filled steel tubes subjected to pure bending.* Journal of Constructional Steel Research, 2009. **65**(8): p. 1836-1845 DOI: https://doi.org/10.1016/j.jcsr.2009.04.006.

[3] Dadfar, B., M. Hesham El Naggar, and M. Nastev, *Ovalization of steel energy pipelines buried in saturated sands during ground deformations.* Computers and Geotechnics, 2015. **69**: p. 105-113 DOI: https://doi.org/10.1016/j.compgeo.2015.05.004.

[4] Sherman, D.R., *Tests of Circular Steel Tubes in Bending.* Journal of the Structural Division, 1976. **102**(11): p. 2181-2195 DOI: https://doi.org/10.1061/JSDEAG.0004478.

[5] Sherman, D.R. *Inelastic flexural buckling of cylinders*. in *International Conference "Steel Structures: Recent Advances and Their Application to Design"*. 1986. Budva, Montenegro: Elsevier.

[6] Schilling, C.G., *Buckling Strength of Circular Tubes.* Journal of the Structural Division, 1965. **91**(5): p. 325-348 DOI: https://doi.org/10.1061/JSDEAG.0001335.

[7] Jirsa, J.O., et al. *Ovaling Of Pipelines Under Pure Bending*. in *Offshore Technology Conference*. 1972.

[8] Korol, R.M. and J. Hudoba, *Plastic Behavior of Hollow Structural Sections.* Journal of the Structural Division, 1972. **98**(5): p. 1007-1023 DOI: https://doi.org/10.1061/JSDEAG.0003221.

[9] Elchalakani, M., X.L. Zhao, and R.H. Grzebieta, *Plastic Slenderness Limits for Cold-Formed Circular Hollow Sections.* Australian Journal of Structural Engineering, 2002. **3**(3): p. 127-141 DOI: https://doi.org/10.1080/13287982.2002.11464900.

[10] Elchalakani, M., X.-L. Zhao, and R. Grzebieta, *Variable amplitude cyclic pure bending tests to determine fully ductile section slenderness limits for cold-formed CHS.* Engineering Structures, 2006. **28**(9): p. 1223-1235 DOI: https://doi.org/10.1016/j.engstruct.2005.10.022.

[11] CEN, *EN 1993-1: Eurocode 3, Design of steel structures, Part 1*. 1993, European Committee for Standardization (CEN).

[12] Standards Australia / Standards New Zealand, *Cold-formed steel structures. AS/NZS 4600:2005*. 2005: Sydney, Australia.
[13] Standards Australia, *Steel structures. AS 4100-1998*. 1998: Sydney, Australia.
[14] AISC, *Load and resistance factor design specification for structural steel buildings. .* 1999, American Institute of Steel Construction Inc.: Chicago, USA.
[15] Zhu, J. and L.-y. Li, *Nonlinear bending of cylindrical shells subjected to transverse loads.* Mechanics Research Communications, 2020. **107**: p. 103561 DOI: https://doi.org/10.1016/j.mechrescom.2020.103561.
[16] Mamalis, A.G., et al., *Deformation Characteristics of Crashworthy Thin-Walled Steel Tubes Subjected to Bending.* Proceedings of the Institution of Mechanical Engineers, Part C: Mechanical Engineering Science, 1989. **203**(6): p. 411-417 DOI: https://doi.org/10.1243/pime_proc_1989_203_135_02.
[17] Yao, Y., W.-M. Quach, and B. Young, *Finite element-based method for residual stresses and plastic strains in cold-formed steel hollow sections.* Engineering Structures, 2019. **188**: p. 24-42 DOI: https://doi.org/10.1016/j.engstruct.2019.03.010.
[18] Singh, R., J. Tiwari, and A. Kumar, *Self-contact in closed and open Kirchhoff rods.* International Journal of Non-Linear Mechanics, 2021. **137**: p. 103786 DOI: https://doi.org/10.1016/j.ijnonlinmec.2021.103786.
[19] Plevris, V. and G. Tsiatas, *Computational Structural Engineering: Past Achievements and Future Challenges.* Frontiers in Built Environment, 2018. **4**(21): p. 1-5 DOI: https://doi.org/10.3389/fbuil.2018.00021.
[20] Plevris, V. and P.G. Asteris, *Modeling of Masonry Failure Surface under Biaxial Compressive Stress Using Neural Networks.* Construction and Building Materials, 2014. **55**: p. 447-461 DOI: https://doi.org/10.1016/j.conbuildmat.2014.01.041.
[21] Asteris, P.G. and V. Plevris, *Neural Network approximation of the masonry failure under biaxial compressive stress*, in *3rd South-East European Conference on Computational Mechanics (SEECCM III)*. 2013: Kos Island, Greece. p. 584-598. DOI: https://doi.org/10.7712/130113.4411.S215.
[22] Asteris, P.G. and V. Plevris, *Anisotropic masonry failure criterion using artificial neural networks.* Neural Computing and Applications, 2017. **28**(8): p. 2207-2229 DOI: https://doi.org/10.1007/s00521-016-2181-3.
[23] Ben Seghier, M.E.A., et al., *Advanced intelligence frameworks for predicting maximum pitting corrosion depth in oil and gas pipelines.* Process Safety and Environmental Protection, 2021. **147**: p. 818-833 DOI: https://doi.org/10.1016/j.psep.2021.01.008.
[24] Ben Seghier, M.E.A., et al., *On the modeling of the annual corrosion rate in main cables of suspension bridges using combined soft computing model and a novel nature-inspired algorithm.* Neural Computing and Applications, 2021. **33**(23): p. 15969-15985 DOI: https://doi.org/10.1007/s00521-021-06199-w.
[25] Ben Seghier, M.E.A., et al., *Hybrid soft computational approaches for modeling the maximum ultimate bond strength between the corroded steel reinforcement and surrounding concrete.* Neural Computing and Applications, 2021. **33**(12): p. 6905-6920 DOI: https://doi.org/10.1007/s00521-020-05466-6.
[26] Ben Seghier, M.E.A., et al., *Simulation of the ultimate conditions of fibre-reinforced polymer confined concrete using hybrid intelligence models.* Engineering Failure

Analysis, 2021. **128**: p. 105605 DOI: https://doi.org/10.1016/j.engfailanal.2021.105605.

[27] Tran, V.-L., D.-K. Thai, and D.-D. Nguyen, *Practical artificial neural network tool for predicting the axial compression capacity of circular concrete-filled steel tube columns with ultra-high-strength concrete.* Thin-Walled Structures, 2020. **151**: p. 106720 DOI: https://doi.org/10.1016/j.tws.2020.106720.

[28] Mai, S.H., et al., *A hybrid model for predicting the axial compression capacity of square concrete-filled steel tubular columns.* Engineering with Computers, 2022. **38**(2): p. 1205-1222 DOI: https://doi.org/10.1007/s00366-020-01104-w.

[29] Solorzano, G. and V. Plevris, *Optimum Design of RC Footings with Genetic Algorithms According to ACI 318-19.* Buildings, 2020. **10**(6): p. 1-17 DOI: https://doi.org/10.3390/buildings10060110.

[30] Ben Seghier, M.E.A., et al., *Novel hybridized adaptive neuro-fuzzy inference system models based particle swarm optimization and genetic algorithms for accurate prediction of stress intensity factor.* Fatigue & Fracture of Engineering Materials & Structures, 2020. **43**(11): p. 2653-2667 DOI: https://doi.org/10.1111/ffe.13325.

[31] Shahin, M. and M. Elchalakani, *Neural networks for modelling ultimate pure bending of steel circular tubes.* Journal of Constructional Steel Research, 2008. **64**(6): p. 624-633 DOI: https://doi.org/10.1016/j.jcsr.2007.12.001.

[32] Basarir, H., M. Elchalakani, and A. Karrech, *The prediction of ultimate pure bending moment of concrete-filled steel tubes by adaptive neuro-fuzzy inference system (ANFIS).* Neural Computing and Applications, 2019. **31**(2): p. 1239-1252 DOI: https://doi.org/10.1007/s00521-017-3108-3.

[33] Breiman, L., *Bagging predictors.* Machine Learning, 1996. **24**(2): p. 123-140 DOI: https://doi.org/10.1007/BF00058655.

[34] Ho, T.K., *The random subspace method for constructing decision forests.* IEEE Transactions on Pattern Analysis and Machine Intelligence, 1998. **20**(8): p. 832-844 DOI: https://doi.org/10.1109/34.709601.

[35] Ben Seghier, M.E.A., D. Höche, and M. Zheludkevich, *Prediction of the internal corrosion rate for oil and gas pipeline: Implementation of ensemble learning techniques.* Journal of Natural Gas Science and Engineering, 2022. **99**: p. 104425 DOI: https://doi.org/10.1016/j.jngse.2022.104425.

[36] Belgiu, M. and L. Drăguţ, *Random forest in remote sensing: A review of applications and future directions.* ISPRS Journal of Photogrammetry and Remote Sensing, 2016. **114**: p. 24-31 DOI: https://doi.org/10.1016/j.isprsjprs.2016.01.011.

[37] Kennedy, J. and R. Eberhart, *Particle swarm optimization*, in *IEEE International Conference on Neural Networks*. 1995: Piscataway, NJ, USA. p. 1942–1948.

[38] Plevris, V. and M. Papadrakakis, *A Hybrid Particle Swarm – Gradient Algorithm for Global Structural Optimization.* Computer-Aided Civil and Infrastructure Engineering, 2011. **26**(1): p. 48-68 DOI: https://doi.org/10.1111/j.1467-8667.2010.00664.x.

[39] Plevris, V., A. Batavanis, and M. Papadrakakis, *Optimum design of steel structures with the Particle Swarm Optimization method based on EC3*, in *3rd International Conference on Computational Methods in Structural Dynamics and Earthquake Engineering (COMPDYN 2011)*. 2011: Corfu, Greece.

[40] Plevris, V., M.G. Karlaftis, and N.D. Lagaros, *A Swarm Intelligence Approach For Emergency Infrastructure Inspection Scheduling*, in *Sustainable and Resilient Critical Infrastructure Systems: Simulation, Modeling, and Intelligent Engineering*, K. Gopalakrishnan and S. Peeta, Editors. 2010, Springer. p. 201-230. DOI: https://doi.org/10.1007/978-3-642-11405-2_8.

[41] Zhu, S.-P., et al., *Hybrid and enhanced PSO: Novel first order reliability method-based hybrid intelligent approaches.* Computer Methods in Applied Mechanics and Engineering, 2022. **393**: p. 114730 DOI: https://doi.org/10.1016/j.cma.2022.114730.

[42] Plevris, V., *Innovative computational techniques for the optimum structural design considering uncertainties*. 2009, National Technical University of Athens: Athens, Greece. p. 312.

[43] Taylor, K.E., *Summarizing multiple aspects of model performance in a single diagram.* Journal of Geophysical Research: Atmospheres, 2001. **106**(D7): p. 7183-7192 DOI: https://doi.org/10.1029/2000JD900719.